

Controls of mass transport deposit and magnetic mineral diagenesis on the sediment magnetic record from the Bay of Bengal

Hilda Maria João¹, Firoz Badesab^{1*}, Virsen Gaikwad¹, Muralidhar Kocherla¹, K. Deenadayalan²

¹ CSIR - National Institute of Oceanography, Dona Paula 403004, Goa, India

² Indian Institute of Geomagnetism, New Panvel, Navi Mumbai, Maharashtra, India

*Corresponding author: Firoz Badesab (firoz@nio.org)

Abstract

We conducted rock magnetic, mineralogical, sedimentological and geochemical analyses on a sediment core (MD161/Stn-11) retrieved from a complex marine sedimentary system of Krishna-Godavari (K-G) basin to delineate the control of mass transport deposits (MTD's) and methane-induced diagenesis on the sediment magnetic record. Four sediment magnetic zones (Z-I, Z-II, Z-III, Z-IV) were defined based on rock magnetic signatures. The sediment magnetic signal is mainly carried by complex magnetic mineral assemblages of detrital (titanomagnetite, titanohematite) and diagenetic (pyrite) minerals. Changes in rock magnetic properties are mainly controlled by fluctuations in supply of detrital magnetic particles, onset of MTD's and differential rate of methane-influenced magnetic minerals diagenesis in the studied sediment core. Downcore reduction in magnetic susceptibility followed by subsequent precipitation of iron sulfides within sediment magnetic zone (Z-I) representing the period of normal sedimentation can be attributed to diagenetic dissolution caused by anaerobic oxidation of methane coupled to sulfate reduction. Decline in magnetic susceptibility and increase in sediment grain size within MTD-rich sediment intervals (Z-II, Z-III, Z-IV) is linked to loss of finer magnetic grains due to diagenetic dissolution and dilution caused by increase in concentration of diamagnetic minerals. Lower values of magnetic grain size diagnostic (ARM/IRM) parameter indicate loss of finer and selective retention of coarser magnetic particles due to diagenetic dissolution beyond 12 mbsf. Elevated content of total organic carbon (TOC) content in Z-III and Z-IV can be attributed to the efficient preservation of labile organic matter due to rapid sediment deposition. A conceptual model is presented to explain the control of mass transport deposit and magnetic mineral diagenesis on the sediment magnetic record.

Key points:

- Delineated the control of geological and methane-induced diagenetic processes on the sediment magnetic record from the Bay of Bengal.
- Established the linkage between sediment magnetism, mass transport deposits, preservation of organic carbon, sediment grain size, and magnetic mineral diagenesis in a rapidly depositing marine sedimentary system.
- A conceptual model summarizing the control of steady and non-steady sedimentation on the sediment magnetic record is developed.

Key words: Rock Magnetism; Magnetic Minerals; Sedimentation; Diagenesis; Methane; Bay of Bengal

1. Introduction

Magnetic iron minerals are ubiquitous and indicative of sedimentary constituents, and their associated magnetic signals provides vital information on the primary depositional and secondary diagenetic processes (Thompson and Oldfield, 1986; Liu et al., 2012;). A wide range of environmental processes imprints distinct changes in the concentration, mineralogy, and grain size of magnetic minerals which can be quantified at high sensitivity using magnetic methods (Evans and Heller, 2003; Liu et al., 2012). Variation in sediment provenance, sedimentation rates, and depositional conditions govern the concentration, mineralogy, and grain size of magnetic particles and could significantly affect the sediment magnetic records (Thompson and Oldfield, 1986). In addition, post-depositional processes including reductive diagenesis, authigenesis and biogenesis can also significantly alter the sediment magnetism (Berner, 1970; Karlin and Levi, 1985; Roberts, 2015; Roberts et al., 2018). Hence, sedimentary magnetic minerals have been utilized as excellent markers to resolve a range of scientific problems including identification of sediment provenance, characterization of depositional environment, tracking the pathways of sediments and pollutants, mapping of magnetite-rich heavy mineral deposits, diagenetic, authigenic and biogenic processes in coastal, continental margin and deep sea sediments (Oldfield et al., 1985; Razjigaeva and Naumova, 1992; Oldfield and Yu, 1994; Lees and Pethick, 1995; Cioppa et al., 2010; Hatfield et al., 2010; Badesab et al., 2012; Dewangan et al., 2013; Roberts, 2015; Hatfield and Maher, 2008, 2009; 2017; 2019).

Diagenesis of magnetic minerals in methanic sediments is controlled by biogeochemical process involving coupled interaction between rising methane flux and downward diffusing sulfate gradients (Knittel and Boetius, 2009). Large amount of hydrogen sulfide generated as a result of anaerobic oxidation of methane reacts with the dissolved iron and produces magnetic iron sulfides (Canfield and Berner, 1987; Riedinger et al., 2005; Kars and Kodama, 2015; Badesab et al., 2017). Rock magnetic properties of sediments from methane-rich and gas hydrate bearing environments has been extensively studied. For example in Bay of Bengal (Dewangan et al., 2013; Badesab et al., 2017; 2019), Nankai trough, Japan (Kars and Kodama, 2015; Shi et al., 2017), continental margin offshore of southwestern Taiwan (Horng and Chen, 2006; Horng, 2018; Horng and Roberts, 2018), Cascadia Margin (Housen and Musgrave, 1996; Liu, 2004; Musgrave et al., 2006; Larrasoana et al., 2007; Esteban et al., 2008; Rowan et al. 2009; van Dongen et al. 2007; Rodelli et al. 2019), continental margin off Argentina and Uruguay (Garming et al., 2005; Riedinger et al., 2005). In a high energy dominated sedimentary system like Krishna-Godavari (K-G) basin, control of sedimentation rate/events or mass transport deposits (MTD's) can significantly affect the diagenesis of magnetic minerals (Riedinger et al., 2005; März et al., 2008; Roberts, 2015). In the K-G basin, several MTDs have been identified in the shallow and

deep offshore regions as confirmed by high-resolution seismic data, multibeam bathymetry, seafloor topography, core lithology, and sediment ages (Ramana et al., 2007; Dewangan et al., 2010; Ramprasad et al., 2011; Yamamoto et al., 2018). A geophysical study by Ramprasad et al. (2011) revealed that neotectonic events, gas hydrate dissociation, sea level variations, and rapid sedimentation events triggered slumping/sliding activities and generated MTDs in the K-G basin. Sediments deposited in the K-G basin very well record the events of higher sedimentation and methane controlled diagenetic changes. So far, rock magnetic studies in the K-G basin mainly focussed on unravelling the complex magnetic mineral assemblages in a gas hydrate bearing sediments (Dewangan et al., 2013; Badesab et al., 2017), establishing the linkages between magnetic mineral diagenesis, cold-seep related processes and evolution of the gas hydrate system (Badesab et al., 2019; 2020). However, a focussed rock magnetic study evaluating the control of MTD's and methane-induced diagenetic processes on the sediment magnetic record was still lacking.

The Krishna-Godavari (K-G) basin represents an ideal natural laboratory to examine the constraints on the evolution of sediment magnetic record. The basin is unique as it receives higher supply of detrital (magnetite-rich) sediment load by Krishna and Godavari river systems (Ramesh and Subramanian, 1988; Sangode et al., 2001), occurrences of MTD's created by rapid sedimentation events, shale-tectonism driven by sliding/slumping activities, sea-level fluctuations, gas hydrate dynamics, complex channel-levee system (Ramana et al., 2007; Ramprasad et al., 2011; Kumar et al., 2014; Collett et al., 2019) and presence of abundant methane and hydrates (Mazumdar et al., 2012; Kumar et al., 2014). Sediment cores collected during a dedicated gas hydrate exploration cruise (MD161) of Council of Scientific and Industrial Research – National Institute of Oceanography (CSIR-NIO) record the signature of geological and geochemical processes in the K-G basin. In this study, we conducted a multi-proxy investigation on a sediment core (MD161/Stn-11) retrieved from complex sedimentary system of the K-G basin to evaluate the influence of geological (more specifically MTD's) and methane-related geochemical processes on the sediment magnetic record.

2. Study area and geology

The Krishna-Godavari (K-G) basin is located along the central east coast of India which extends from Ongole in the south to Vishakhapatnam in the north. It covers an onshore area of about 28,000 km² and extends to the offshore area of 145,000 km² (Rao 2001; Ojha and Dubey, 2006;). The detrital bulk sediment load mainly consists of montmorillonite clay with traces of illite and kaolinite supplied by the Krishna and Godavari rivers. In addition, Ganges–Brahmaputra river systems also supply sediments to the K-G basin which are mostly coarse grained and comprised of illite, kaolinite, and chlorite (Gibbs, 1977; Subramanian, 1980). The average thickness of deposited sediment in the K-G

basin varies from 3 to 5 km in the onshore and 8 km in the offshore region respectively (Prabhakar and Zutshi, 1993). Previous geophysical studies reported the presence of various structures in the study area including bathymetric mounds, deep-seated shale diapirs and toe thrust faults formed due to shale tectonism/neotectonism (Ramana et al., 2007; Dewangan et al., 2010).

3. Materials and methods

As a part of CSIR-NIO's gas hydrate exploration program, a 28.1 m long sediment (gravity core, MD161/Stn-11) overlying the methane hydrate deposits was retrieved onboard R/V Marion Dufresne (Cruise no: MD161) from the K-G basin in May 2007 (Fig. 1). The location of the sediment core (MD161/Stn-11) lies in mid-slope region of the K-G offshore basin. The sediments comprised of greenish gray to olive green colored clay-rich in core MD161/Stn-11. Bulk sediment grain size is dominated by silt and clay sized fractions (Fig. 2g). Authigenic carbonates of various size and morphology were noticed beyond 10 mbsf in the core (Fig. 7). The sediment lithology mainly composed of nannofossil and foraminifera bearing clay. Dead shells and gastropods were found throughout in MTD rich (> 12 mbsf) sediment intervals. This core has been extensively studied for reconstruction of paleomagnetic secular variation (Usapkar et al., 2016), sediment pore fluid compositions to develop possible linkage with sub-surface gas hydrate deposits (Mazumdar et al., 2012), composition and stable carbon and oxygen isotopes of authigenic carbonates to gain insights into the highly dynamic biogeochemical process (Kocherla et al., 2015) and radiocarbon dating study for understanding sliding/slumping activities in the K-G basin (Ramprasad et al., 2011). The present day sulfate methane transition zone (SMTZ) in core MD161/Stn-11 is identified between 5 – 6 mbsf based on the pore water profiles of sulfate and methane concentration (Mazumdar et al., 2012). Highest values of total alkalinity are seen at present day SMTZ and showed further downcore increase upto bottom of Z-II (Fig. 2i).

3.1. Sampling and measurements

The sediment core (MD-161/Stn-11) was sub-sampled at 5 cm intervals. For magnetic analysis, 321 sub-samples were dried, weighed, and packed in a 25 mm cylindrical plastic sample bottles. Measurements were carried out at the Paleomagnetic laboratory of CSIR-NIO, Goa, India.

3.2. Age model

Age-model based on radiocarbon dating for the sediment core MD161/Stn-11 was established by Ramprasad et al. (2011). AMS ^{14}C dates of planktonic foraminifera revealed a uniform sedimentation rate of 2.1 m/kyr in the topmost (<12 mbsf) part of the sediment core (Table 1). The sedimentation

rate increases significantly to >40 m/kyr below 12 m, and age reversal is noticed in this core which further provides direct evidence of MTD's at this site.

3.3. Rock magnetic analysis

Using a Bartington Instruments MS2B dual frequency susceptibility meter magnetic susceptibility (χ) measurements were performed. The susceptibility was measured at two different frequencies $\chi_{lf} = 0.47$ kHz and $\chi_{hf} = 4.7$ kHz. Frequency dependent magnetic susceptibility was calculated as $\chi_{fd} \% = (\chi_{lf} - \chi_{hf}) / \chi_{lf} \times 100$. Anhysteretic remanent magnetization (ARM) was applied using a 100 mT alternating field (AF) field with a superimposed fixed direct current (DC) bias field of 50 μ T and was measured using a AGICO JR-6A spinner magnetometer. Mass-normalized ARM Susceptibility is calculated as divided by the DC bias field. By using a MPM10 pulse magnetizer, isothermal remanent magnetization (IRM) was applied in an inducing field of +1T in the forward direction and was demagnetized by DC backfields at -20 mT, -30 mT, -100 mT and -300 mT. The respective remanence was measured using AGICO JR-6A spinner magnetometer. The saturation isothermal remanent magnetization (SIRM) is considered to be mass-normalized IRM acquired at a peak field of 1T. S-ratio is calculated as the ratio between the IRM at -300 mT and SIRM ($IRM_{-300mT}/SIRM_{1T}$) (Thompson and Oldfield, 1986).

Thermomagnetic measurements were conducted at Indian Institute of Geomagnetism, Panvel, India. Magnetization was measured in a field of 300 A/m at 875 Hz by a CS-3 furnace unit coupled to an AGICO (KLY-4S) Kappabridge. The high temperature measurements were performed from room temperature to 700°C in argon atmosphere.

3.4. Sedimentological analyses

3.4.1. Grain size measurements

Sediment grain size measurements were carried out using a Malvern Mastersizer 2000 laser particle size analyzer at CSIR-NIO, Goa, India. Samples were first desalinated and later decarbonised using dilute HCl (1N). To remove organic carbon sediment suspensions were treated with 10% H₂O₂ and the dispersing agent Sodium hexa-meta phosphate was added to the suspension, and ultrasonicated prior to analysis. Sediment mean grain size values presented in this study are in μ m.

3.4.2. Mineralogical analysis

Magnetic particles were separated by following the extraction method proposed by Petersen et al. (1986) from the bulk sediment samples. Using a scanning electron microscope (SEM) (JEOL JSM-5800 LV) Images of magnetic particles were captured in secondary electron (SE) imaging mode at

energy levels between 15 and 20 keV. The composition of magnetic particles was determined using an energy dispersive X-ray spectroscopy (EDS) probe attached to the microscope. The magnetic mineralogy of representative samples from a sediment core was determined using a Rigaku X-Ray Diffractometer (Ultima IV) at CSIR-NIO, Goa, India. The samples were run from 15° to 70° of 2 θ at 1°/min scan speed using Cu K α radiation ($\lambda = 1.5414 \text{ \AA}$).

3.5. Geochemical analyses

Geochemical analyses were carried out at CSIR-NIO, Goa, India. Total carbon (TC) content of sediments was measured by elemental analyzer (Thermo/Carbo Erba NA). The instrument was calibrated using NC soil standard. Analytical precision achieved was <2% for the TOC measurements. Total inorganic carbon (TIC) content was measured by UIC carbon coulometer (CM 5130). The accuracy of TIC content of standard reference material (CaCO₃, Sigma-Aldrich) was within $\pm 2\%$. Total organic carbon (TOC) was calculated by subtracting TIC from TC. Pore-water geochemical data and methane concentrations of core MD161/Stn-11 was taken from Mazumdar et al. (2012). For determination of iron (Fe) concentration, dried bulk sediment samples were digested with hydrofluoric acid (HF), perchloric acid (HClO₄) and nitric acid (HNO₃). Fe concentrations were measured on a Perkin-Elmer Optima 2000 ICP-OES.

4. Results

4.1. Downcore rock magnetic property variations

We broadly classified the rock magnetic profile of the sediment core MD161/Stn-11 into four sediment magnetic zones: Z-I (0.22 – 10.92 mbsf), Z-II (11.07 – 13.97 mbsf), Z-III (14.02 – 17.87 mbsf), and Z-IV (17.97 – 28.02 mbsf) based on the downcore changes in the magnetic mineral concentration, composition and granulometry data (Fig. 2a, b, c, d). A gradual down-core decrease in χ_{lf} , ARM, SIRM is noticed in Z-I (Fig. 2a, b, c). Magnetic grain size diagnostic proxy (ARM/SIRM) showed variations in all four sediment magnetic zones (Fig. 2d). Low and high values of ARM/SIRM within Z-I indicate the dominance of finer as well as coarser magnetic particles (Fig. 2d). S-ratio in Z-I varies between 0.93 – 0.99 indicating that dominant magnetic mineralogy in Z-I is possessed by ferrimagnetic minerals (Fig. 2e). In Z-II, a distinct drop in χ_{lf} , ARM, SIRM and lowest ARM/SIRM values in Z-II reflects the decrease in concentration of coarser magnetic particles (Fig. 2a,b,c,d). S-ratio in Z-II varies between 0.94 – 0.99 (Fig. 2e). In Z-III, we noticed an initial rise in χ_{lf} , ARM, SIRM and ARM/SIRM values relative to Z-II and Z-IV indicating slight increase in concentration of fine-grained magnetic particles (Fig. 2a,b,c,d). S-ratio in Z-III varies between 0.93 – 0.99 (Fig. 2e). Z-IV is marked by lower χ_{lf} , ARM, SIRM than Z-I indicating substantial decrease in magnetic mineral concentration.

ARM/SIRM values in Z-IV is slightly higher than Z-II (Fig. 2d). S-ratio in Z-IV varies between 0.93 – 0.99 (Fig. 2e). A trend of down core increase in TOC and mean grain size is observed in Z-I (Fig. 2f, g). While an opposite trend showing decrease in TOC and increase in mean grain size is noticed in Z-II (Fig. 2f, g). A noticeable increase in TOC accompanied by slight rise in mean grain size values is seen in Z- III (Fig. 2f, g). Z-IV showed less variation in TOC, but exhibited mixed trend in mean grain size values (Fig. 2f, g).

4.2. X-ray diffraction (XRD) analysis on magnetic separates

Titanomagnetite is the major magnetic mineral identified in all sediment magnetic zones of core MD161/Stn-11 (Fig. 3a-h). In addition, we also noticed the presence of quartz (Fig. 3a,b,c,d,e,g,h), pyrite (Fig. 3b-h) and rutile (Fig. 3b,c,d,g) in all four sediment magnetic zones.

4.3. Scanning electron microscopy (SEM) and energy dispersive spectrum (EDS) analyses of magnetic particles

SEM-EDS results indicate that the titanomagnetite is the dominant magnetic mineral in the studied sediment core (Fig. 4a-j). We noticed numerous well-preserved as well as altered titanomagnetite grains of different sizes and shapes (Fig. 4a-j). Z-I is dominated by fine-coarse grained titanomagnetites (Fig. 2a, b). We observed a skeletal type Ti-rich grain (titanohematite), with quadrangle plate-like structure exhibiting the dissolution features observed in Z-II (Fig. 4d; Nowaczyk, 2011; Poulton et al., 2004). Numerous well-developed pyrite framboids and detrital titanomagnetites are observed in Z-III and Z-IV (Fig. 4e-j).

4.4. Correlation between magnetic, sedimentological and geochemical parameters

Bivariate plots between magnetite concentration (χ_{lf} , SIRM) and grain size ($\chi_{fd\%}$, ARM/SIRM) dependent, sedimentological (mean grain size) and geochemical (TOC, Fe) parameters are presented in Fig. 5a-f. A trend of coarsening in magnetic grain size is observed more specifically in samples from Z-I. Finer magnetic particles showed higher values of χ_{lf} (Fig. 5a). Samples from other zones (Z-II, Z-III, Z-IV) did not exhibit any clear trend and showed relatively lower χ_{lf} and dominance of fine as well as coarser magnetic minerals (Fig. 5a). A positive correlation ($R^2 = 0.80$) between χ_{lf} and SIRM for all samples indicate that the major magnetic mineralogy is dominated by ferrimagnetic minerals (Fig. 5b). A positive correlation ($R^2 = 0.71$) between χ_{lf} and ARM/SIRM is seen (Fig. 5c). Higher susceptibility is dominated by fine-grained magnetic particles and vice versa (Fig. 5c).

Cross plot between χ_{lf} and mean grain size showed modest relationship. Z-I samples showed finer grain size ($< 5.5 \mu\text{m}$) with high χ_{lf} , while the samples from Z-II, Z-III and Z-IV are relatively coarser ($> 5.6 \mu\text{m}$) and exhibit lower χ_{lf} (Fig. 5d). We observed good correlation ($R^2 = 0.40$) between χ_{lf} and TOC

parameters for all zones (Fig. 5e). Samples with high TOC (Z-II, Z-III, Z-IV) showed low χ_{lf} values, while Z-I samples showed relatively high χ_{lf} and low TOC values (Fig. 5e). It is interesting to note that samples from Z-I showed wide range in TOC and χ_{lf} values (Fig. 5e). A positive correlation ($R^2 = 0.70$) between χ_{lf} and Fe content is observed in Z-I samples, while other zones (Z-II, Z-III, Z-IV) showed much lower and narrow range in Fe and χ_{lf} values (Fig. 5f).

4.5. Thermomagnetic experiments

Thermomagnetic analyses on the representative sediment samples covering all sediment magnetic zones (Z-I, Z-II, Z-III, Z-IV) are presented in Fig. 6. A significant drop in magnetization is observed between 563°C and 595°C indicating that dominant magnetic mineralogy of the bulk sediments is titanomagnetite (Fig. 6a-e). A minor increase in χ between 332°C and 480°C is mainly due to the transformation of paramagnetic minerals into magnetite because of the heating process (Hirt et al., 1993; Passier et al., 2001).

5. Discussion

5.1. Magnetic mineral assemblages in MTD-rich sediment intervals of core MD161/Stn-11

High resolution geophysical study carried out by Ramprasad et al. (2011) provided evidence of MTDs generated by slumping and sliding activities triggered by neotectonism at the studied site. Radiocarbon dating indicated that normal and uniform sedimentation continued in the upper 12 mbsf with a sedimentation rate of 2.1 m/kyr, while below 12 mbsf enhanced increase in sedimentation upto >40 m/kyr was reported at this site (Ramprasad et al., 2011). An age reversal at 15 mbsf and abrupt sedimentation rate below 12 mbsf provided convincing evidence on the occurrence of MTDs at the studied site (Ramprasad et al., 2011). In the studied core, sediment magnetic zone Z-I corresponds to normal sedimentation (upper 12 mbsf) and Z-II, Z-III, Z-IV represents MTD-rich sediment (below 12 mbsf) intervals (Ramprasad et al., 2011; Mazumdar et al., 2012). Concerning the primary source of magnetic minerals, detrital magnetic grains supplied via terrigenous sources are the main contributors affecting the bulk sediment magnetic susceptibility signal in the studied samples (Sangode et al., 2001; Phillips et al., 2014). Based on the rockmagnetic mineralogy diagnostic parameters (S-ratio), thermomagnetic curves coupled with XRD and SEM-EDS data, we confirmed that the titanomagnetite (detrital origin) dominates the bulk sediment magnetic signal (Fig. 2e, Fig. 3a-h, Fig. 4a-i, Fig. 6a-e). Fluctuations in monsoonal conditions, intensities of weathering and erosional processes in peninsular India, and glacial/interglacial cycles significantly affected the delivery of detrital sediment load to the K-G basin (Colin et al., 1999; Sangode et al., 2001; Krishna et al., 2016). Krishna and Godavari rivers flow through the Deccan Traps basalts and Precambrian metamorphic rocks and supply sediments

from these terrains into the K - G basin (Ramesh and Subramanian, 1988). The sediment core (MD161/Stn-11) preserves a good record of sedimentary deposits (MTD's) and related processes in the basin. A large flux of magnetite-rich detrital load delivered by the Krishna and Godavari river system yielded high magnetic mineral concentration as seen through higher values of χ_{lf} , ARM, SIRM in Z-I (Fig. 2a, b, c). A positive correlation ($R^2 = 0.80$) between χ_{lf} and SIRM indicates that rock magnetic parameters of core MD161/Stn-11 are mainly controlled by the varying contribution of ferrimagnetic minerals (Fig. 2a,c and Fig. 6). Higher magnetite concentration in Z-I also provide clues on the intense weathering and erosional processes in the hinterlands and higher river run off which enhanced the sediment supply to the K-G basin during the formation of Z-I.

Bulk sediment magnetic signal in marine sediment is strongly affected by dilution with paramagnetic and diamagnetic minerals (Mohamed et al., 2017). The distinct drop in concentration dependent magnetic parameters in MTD-rich sediment intervals below 12 mbsf (Z-II, Z-III, Z-IV) could be either due to intense sediment mixing and reworking triggering by sliding/slumping activities (Ramprasad et al., 2011), or dilution caused by increased terrigenous (diamagnetic) inputs or due to different sediment provenance and age. We proposed that distinct drop in χ_{lf} within the MTD-rich sediment intervals (below 12 mbsf) could be due to the dilution of ferromagnetic minerals caused by increase in the concentration of diamagnetic and paramagnetic minerals like quartz and clay. Our interpretation is similar to the observations reported in sediments from Galician Rias Baixas (Mohamed et al., 2017), and Ria de Pontevedra, NW Spain (Rey et al., 2005).

In rapidly depositing marine sedimentary systems, sedimentation rates, oxygen concentration, and rates of oxic and suboxic processes control the preservation of TOC (Calvert and Pedersen, 1993; Nagoji, 2017). A dedicated sediment geochemistry study on marine sediment cores from the K-G basin by Mazumdar et al. (2012) reported that MTDs are a potential source of methane gas as the quick deposition of sediment would enhance the preservation of labile organic matter which will subsequently undergo bacterial mineralization and generate methane and carbon dioxide. Intense sediment mixing and reworking in MTD intervals triggered by sliding/slumping activities (Ramprasad et al., 2011) might have affected the oxidation of labile organic matter and thereby reduced the rate of remineralization and subsequently delayed the sulfidic diagenetic processes (Rey et al., 2005). In the studied sediment core, downcore increase in TOC and mean sediment grain size followed by reduction in χ_{lf} in MTD-rich sediment intervals is noticed (Fig. 2a,f,g). Higher TOC content in Z-III and Z-IV can be attributed to the efficient preservation of labile organic matter due to rapid sediment deposition (Fig. 2f). Reduction in χ_{lf} with increase in sediment grain size in Z-II, Z-III, Z-IV could be due to dilution effect caused by increase in concentration of diamagnetic minerals (Fig. 2a,g). The presence

of abundant quartz through the core supports our interpretation (Fig. 3a-h and Fig. 4a-j). Similar observations were reported in sediments from Ria de Muros, NW Iberia (Mohamed et al., 2005) and Rias Baixas, NW Spain (Vilas et al., 2005).

5.2. Magnetic mineral transport, sorting and burial in MTDs

Rock magnetic sediment record of core MD161/Stn-11 retrieved from a MTD-prone region of K-G basin provides an excellent opportunity to examine the dynamics (transport, sorting and burial) of magnetic particles during their deposition in normal (Z-I) and rapidly deposited (Z-II, Z-III, Z-IV) sediments. Changes in the concentration and grain size of magnetic particles suggests that the sedimentation of two distinct intervals (a) top 10.92 mbsf (Z-I) and (b) 11.07 mbsf - 28.02 mbsf (Z-II, Z-III, Z-IV) must have taken place under very different morphodynamic conditions. Distinct magnetic zonation between Z-I and other zones Z-II, Z-III, Z-IV indicate differences in their depositional mechanism (Fig. 2a-d). As seen through ARM/SIRM values, differences in the magnetic grain-size between Z-I (mixture) and Z-II, Z-III, Z-IV (coarser) could be linked with the specifics of the sediment dynamics during each depositional event. We hypothesize that rapid burial of coarser magnetic grains driven by gravitation settling during each MTD event might have created such differences in magnetic grain size (Fig. 2d; Gallaway et al., 2012; Badesab et al., 2017). A sudden drop in magnetic grain size diagnostic (ARM/SIRM) proxy in Z-II and Z-IV could also be due to the diagenetic dissolution of finer and preservation of coarser magnetic particles in Z-II and Z-IV (Fig. 2d; Dillon and Bleil, 2006; Dewangan et al., 2013).

In Z-I, we hypothesize that relatively calmer condition and normal sedimentation (Ramprasad et al., 2011) persisted which allowed sufficient time for the settling of fine and coarser magnetic particles during its formation (Fig. 2d). ARM/SIRM profile showed the presence of finer as well as coarser magnetic particles in Z-I (Fig. 2d). It is interesting to note that the fine grained magnetic particles dominate in Z-I compared to all other sediment magnetic zones (Fig. 2d). This observation suggests that the differential mechanism controlled the settling and transport of fine and coarser magnetic particles in these zones. In addition to diagenetic effect, upward fining (as evident through increase in ARM/SIRM values from 8.5 mbsf to 2.0 mbsf in Z-I) in magnetic grain size also provides clue on the hydrodynamic sorting process which might have favoured the deposition of finer magnetic particles during that period (Fig. 2d). These observations explain the linkage between dynamics (sorting, burial, transport) of magnetic particles and variations in bulk sediment magnetic signal. A good covariation between mean grain size and χ_{lf} suggests that sediment deposition in the MTD rich sediment intervals (Z-II, Z-III, Z-IV) is also controlled by differences in hydraulic behaviour driven by the density and grain size of magnetic minerals (Fig. 5d). Downcore increase in mean grain size (physical)

accompanied by presence of coarser magnetic grains (as indicated by lower ARM/SIRM values) in Z-II, Z-III, and Z-IV provides direct evidence on hydraulic sorting of magnetic minerals within MTD-rich sediment intervals at site MD161/Stn-11 (Fig. 2a, d, g). The observed linkages between sediment magnetic signals and the processes controlling the dynamics of magnetic particles signifies the importance of using magnetic methods to track the transport and depositional dynamics of magnetic particles in a normal as well as rapidly depositing sedimentary system.

5.3. Control of methane influenced diagenetic disturbances on the sediment magnetism

Diagenetic alteration created by methane induced biogeochemical processes can significantly modulate the sediment magnetic record by altering the primary and creating the secondary magnetic phases (Roberts, 2015). In this section, we evaluate the influence of methane-related diagenetic processes on the rock magnetic properties of sediment core MD161/Stn-11 in the K-G basin. Presence of complex magnetic mineral assemblages (titanomagnetite, titanohematite, and pyrite) in the studied core samples explain the variation in magnetic signals in each sediment magnetic zone (Fig. 2, Fig. 3, Fig. 4). Changes in rock magnetic parameters, XRD, SEM-EDS data and pore-water geochemical (sulfate, methane) profiles helped to examine the magnetic mineral diagenesis in different sediment magnetic zones (Fig. 2, Fig. 3, Fig. 4). For example, fluctuations in χ_{lf} throughout the core provides clue on the subtle variations in the supply of detrital magnetite-rich sediments to the K-G basin (Fig. 2a). A drop in χ_{lf} and SIRM manifested by the presence of pyrite just below present-day SMTZ can be attributed to the intense pyritization fuelled by AOM-coupled sulfate reduction in the studied core (Fig. 2a,c,h,j). Multiple χ_{lf} drops at different depth intervals in all four sediment magnetic zones hint on the temporal build-up and rapid migration of paleo-SMTZ fronts. It is highly likely that abrupt sedimentation driven by MTD's might have significantly affected paleo-SMTZ fronts formed due to short-lived AOM-coupled sulfate reduction which controlled the magnetic mineral diagenesis mainly in Z-II, Z-III, and Z-IV.

In marine sedimentary system, supply of organic matter, availability of reactive iron and sulfate concentration are three major drivers that constrain the formation of iron sulfide minerals (Berner, 1984; Roberts, 2015). Higher TOC content and increase in sediment grain size within MTD-rich sediment intervals accompanied by down core decrease in χ_{lf} in Z-III and Z-IV suggest that enhanced sedimentation during this periods facilitated rapid burial and preservation of organic matter (Fig. 2a, f, g). In the studied core, the sediment grain size varies between 3.33 μm - 8.12 μm which corresponds to clay and very fine silt fraction (Fig. 2g). Association between high TOC preservation in silt and clay fraction is well-known as organic matter preferentially tends to adhere on the finer fraction, due to increased sorptive capacity of smaller particles with large specific surfaces (Mayer et al., 1985; Keil

et al., 1994; Mohamed et al., 2017). This observation explain the linkage between sediment grain size and preservation of TOC in MTD-rich intervals. A skeletal type titanohematite grain exhibiting the dissolution features is observed in Z-II (Fig. 4d). Slight decrease in S-ratio and χ_{lf} values in Z-II can be attributed to the minor presence of highly coercive magnetic (titanohematite) grains of detrital origin which survived the diagenetic attack by offering resistant to hydrogen sulfide dissolution and therefore remain preserved (Garman et al., 2005).

In marine sediments, rate of dissolution of magnetic minerals increases with increase in TOC content (Moreno et al., 2008). We observed good correlation ($R^2 = 0.40$) between χ_{lf} and TOC parameters for all zones (Fig. 5e). Samples possessing high TOC content showed lower χ_{lf} and vice-versa (Fig. 5e). We propose that presence of high TOC content and increased methane production provided conducive geochemical environment favouring diagenesis of magnetic minerals. These led to subsequent transformation of iron oxides into iron sulfides (Canfield and Berner, 1987). Presence of pyrite in Z-III (16.00 mbsf) and Z-IV (27.65 mbsf) accompanied by low χ_{lf} provides evidence for our hypothesis (Fig. 4e,j). χ_{lf} reduction in MTD-rich intervals (Z-II, Z-III, Z-IV) is most likely controlled by the combined effect of dilution of ferromagnetic minerals caused by increase in concentration of diamagnetic minerals and methane-induced diagenesis. Lower values of ARM/SIRM in Z-II, Z-III, and Z-IV could be attributed to the diagenetic dissolution of finer and preservation of coarser magnetic grains in these zones. In addition to post-depositional methane-influenced diagenetic processes, supply of detrital (magnetite-rich) sediment load could also affect the χ_{lf} record. Bivariate plot between Fe content and χ_{lf} showed two distinct groupings (Fig. 5f). Sediment magnetic zones Z-II, Z-III, Z-IV possessed lower Fe content and exhibit lower susceptibilities in narrow range, while samples from Z-I showed higher Fe content, χ_{lf} and larger scattering (Fig. 5f). These observations indicates that variations in rock-magnetic properties of sediment core MD161/Stn-11 are controlled by variability in supply of magnetic particles, preservation conditions (due to rapid burial, mixing and reworking controlled by MTD's) as well as differential (early versus late) rate of diagenesis in Z-I and Z-II, Z-III, Z-IV respectively. In the studied core, we expected that non-steady state diagenetic processes created by MTD's could significantly alter and preserve the detrital magnetic particles in methanic sediment magnetic zones (Z-II, Z-III, Z-IV). XRD and SEM-EDS data suggest the presence of abundant coarse-grained titanomagnetite (Figs. 3d-h; Figs. 4c,d,f,g,h,i) and skeletal type titanohematite (Fig. 4d) in Z-II, Z-III, and Z-IV. The survival and preservation of these minerals in MTD-rich sediment magnetic zones i.e., below 12 mbsf (Z-II, Z-III, Z-IV) can be explained by the fact that titanohematite and titanomagnetite are more stable and offers strong resistance to reductive dissolution induced by late diagenetic processes (Poulton et al., 2004; Nowaczyk, 2011) or due to rapid

burial because of increased sedimentation in the K-G basin (Riedinger et al., 2005; Badesab et al., 2019; Amiel et al., 2020). Similar observations were made in Niger deep sea fan sediments (Dillon and Bleil, 2006) and Argentine continental slope (Garming et al., 2005).

Based on the rock magnetic, grain size, mineralogical and pore-water geochemical signatures recorded in core MD161/Stn-11, a conceptual model is developed to constrain the influence of steady (normal) and non-steady (rapid) sedimentation processes on the sediment magnetic record (Fig. 7). Onset of high sedimentation events triggered by large scale MTD's delivered huge amount of sediment load to the K-G basin. Lower magnetic susceptibility in MTD-rich sediment intervals (Z-II, Z-III, Z-IV) was either due to the dilution of ferromagnetic minerals caused by increased concentration of diamagnetic minerals or because of intense sediment mixing and reworking triggered by sliding/slumping activities (Ramprasad et al., 2011). Elevated TOC content in Z-III and Z-IV was attributed to the efficient preservation of labile organic matter which survived oxidation due to rapid sediment deposition. Reduction in magnetic susceptibility and increase in sediment grain size in Z-II, Z-III, and Z-IV is linked to the loss of finer magnetic particles due to diagenetic dissolution and dilution caused by increase in concentration of diamagnetic minerals. A close linkage between increase in sediment grain size and TOC content in MTD-rich intervals can be explained based on the fact that organic matter preferentially adhered on the finer (clay to very fine silt) fractions, due to increased sorptive capacity of smaller particles with large specific surfaces and therefore remain preserved (Keil et al., 1994; Mohamed et al., 2017). Non-steady state diagenetic processes created by rapidly deposited sediments favored the rapid burial and preservation of detrital magnetic particles in methanic sediment magnetic zones (Z-II, Z-III, and Z-IV). Titanohematite and titanomagnetite offered strong resistance to reductive dissolution induced by late diagenetic processes and remain preserved in MTD-rich sediment intervals as confirmed through XRD and SEM-EDS data. Z-I highlights the scenario of the normal sedimentation and geochemical conditions leading to diagenesis of magnetic minerals. Detrital minerals supplied by Krishna and Godavari river systems reacted with hydrogen sulfide produced by microbial activity via decomposition of organic matter and AOM-coupled sulfate reduction in Z-I. These resulted in dissolution of detrital Fe-Ti bearing minerals followed by subsequent precipitation of iron sulfides marked by gradual decrease in magnetic susceptibility in Z-I.

6. Conclusion

We present rock magnetic, sedimentological, mineralogical and geochemical records of a sediment core (MD161/Stn-11) that archives signature of mass transport deposits and methane-influenced magnetic mineral diagenesis in the K-G basin, Bay of Bengal. Four distinct sediment magnetic zones comprised of detrital (titanomagnetite, titanohematite) and diagenetic (pyrite) are identified. The

magnetic mineralogy of different sediment magnetic zones has been confirmed by rock magnetic, XRD, and SEM-EDS data. Variations in rock-magnetic properties of the sediment core are controlled by changes in the supply of magnetic particles, preservation conditions (rapid burial, mixing and reworking controlled by MTD's) as well as differential (early versus late) rate of methane-influenced magnetic minerals. Influence of non-steady state sedimentation (MTD's) processes on the sediment magnetic signal (enhancement/depletion), TOC preservation and sediment grain size in the K-G basin has been investigated. A conceptual model (Fig. 7) summarizing the control of steady and non-steady sedimentation on the sediment magnetic record is developed.

Acknowledgement

We thank the Directors of CSIR-NIO, NIOT, NCPOR and advisor MOES for supporting this study. In-charge on-board operations of IPEV are thanked for providing onboard technical support and facilities. We thank Rahul Mohan, Valency and Sahina Gazi from NCPOR and Areef Sardar from CSIR-NIO for providing support to perform SEM-EDS analysis. Girish Prabhu and Prakash Babu are thanked for extending technical support for XRD and organic carbon analysis. We thank Maria Brenda Mascarenhas, Pawan Dewangan, Aninda Mazumdar and T. Ramprasad for providing timely inputs. We thank students of Goa University, IIT Kharagpur and project scientists of CSIR-NIO, NIOT, PRL and CSIR-NGRI. We thank Shanu Cheriyan, Mohamed Mahsoom, Manisha M, Christeena Babu, Abhilash Nandan, Pratha S, Krishnendu K, Godwin Fernandes, and Pooja Satardekar for participating in sub-sampling of sediment core and their valuable contribution during sample analysis. We thank Director, Indian Institute of Geomagnetism (IIGM), Panvel for allowing us to carry out thermomagnetic measurements at the environmental magnetic laboratory. The data used in this study can be made available upon email request to the corresponding author (firoz@nio.org). We sincerely acknowledge the comments/suggestions from Editor (Luigi Tosi), Steve Phillips and two anonymous reviewers. The authors declare no conflicts of interests. This is the contribution of a CSIR-NIO with publication no. xxxx.

Figure caption:

Fig. 1. Location map of sediment core MD-161/Stn-11 in the Krishna-Godavari (K-G) basin, Bay of Bengal. Star (red color) indicates location of sediment core (MD161/Stn -11; present study). Field circle (black color) indicates location of sediment cores retrieved during national gas hydrate expedition (NGHP) -01 and Marion Dufresne (MD) cruise 161. Bathymetry data of the studied area was obtained from GEBCO Compilation Group (2020) GEBCO 2020 Grid (doi: 10.5285/a29c5465-b138-234d-e053-6c86abc040b9). The depth contours are marked by black lines.

Fig. 2. Down-core variations of magnetic (a-e), total organic carbon (TOC) (f), mean grain size (g) and porewater (h-j) data for sediment core MD-161/Station-11. The sedimentary magnetic zones are color coded based on magnetic susceptibility variations. Z-I is marked by pink colour, Z-II is marked by blue colour, Z-III is marked by orange colour and Z-IV is marked by purple colour (a-g). The porewater sulfate profile is marked in red colour, methane profile marked in blue and total alkalinity is marked by green colour (i-j). The present-day depth of sulfate-methane transition zone (SMTZ) is marked.

Fig 3. XRD spectra for minerals extracted from different sediment magnetic zones of sediment core MD161/Stn-11 are shown: (a-c) Z-I, (d) Z-II, (e) Z-III, (f-h) Z-IV. TM: titanomagnetite, P: pyrite, Qz: quartz, R: rutile.

Fig. 4. Scanning electron microscope images (secondary electron images) on magnetic extracts from different sediment magnetic zones of sediment core MD161/Stn-11 Zones: (a-b) Z-I, (c-d) Z-II, (e-g) Z-III, (h-j) Z-IV. EDS spectra are placed adjacent to the respective images. Iron (Fe), titanium (Ti), sulfur (S), oxygen (O), calcium (Ca), silicon (Si), carbon (C), aluminium (Al), magnesium (Mg), and chromium (Cr) peaks are indicated. Please note that the EDS spots on the grains are marked in blue.

Fig. 5. (a-f): Bivariate plots of magnetic susceptibility (χ_{lf}) versus (a) χ_{fd} %, (b) SIRM (c) ARM/SIRM, (d) mean grain size (e) total organic carbon, (f) Fe% for samples from core MD161/Stn-11. Please note that the gray arrows in the scatter plots are used only to highlight the trends.

Fig. 6. (a-e): Thermomagnetic curves of representative samples covering all sediment magnetic zones (Z-1, Z-II, Z-III, Z-IV) in core MD161/Stn-11.

Fig. 7. A conceptual model explaining the different controls influencing the sediment magnetic record at site MD161/Stn-11.

Table. 1. Calendar age of a sediment core (MD161/Stn-11; Ramprasad et al., 2011) situated in the mid-slope region of K-G offshore basin.

References

- Amiel N., Shaar R., Sivan O. (2020). The Effect of Early Diagenesis in Methanic Sediments on Sedimentary Magnetic Properties: Case Study From the SE Mediterranean Continental Shelf. *Frontiers in Earth Science*. <https://doi.org/10.3389/feart.2020.00283>
- Badesab F, Dewangan P, Gaikwad V. (2020). Magnetic mineral diagenesis in a newly discovered active cold seep site in the Bay of Bengal. *Frontiers in Earth Science*. <https://doi.org/10.3389/feart.2020.592557>
- Badesab F, Dewangan P, Gaikwad V, Kars M, Kocherla M, Krishna KS, Sangode SJ, Deenadayalan K, Kumar P, Naikgaonkar O, Ismaiel M. (2019). Magnetic mineralogical approach for the exploration of gas hydrates in the Bay of Bengal. *Journal of Geophysical Research: Solid Earth*. *124*(5), 4428-4451. <https://doi.org/10.1029/2019JB01746>
- Badesab, F., Dewangan, P., Usapkar, A., Kocherla, M., Peketi, A., Mohite, K., et al. (2017). Controls on evolution of gas-hydrate system in the Krishna-Godavari basin, offshore India. *Geochemistry, Geophysics, Geosystems*, *18*, 52–74. <https://doi.org/10.1002/2016GC006606>
- Badesab, F., von Dobeneck, T., Bryan, K. R., Müller, H., Briggs, R. M., Frederichs, T., & Kwohl, E. (2012). Formation of magnetite-enriched zones in and offshore of a mesotidal estuarine lagoon: An environmental magnetic study of Tauranga Harbour and Bay of Plenty, New Zealand. *Geochemistry, Geophysics, Geosystems*, *13*(6). <https://doi.org/10.1029/2012GC004125>
- Berner, R. A. (1970). Sedimentary pyrite formation. *American Journal of Science*, *268* (1), 1–23.
- Berner, Robert A. (1984): "Sedimentary pyrite formation: an update." *Geochimica et Cosmochimica Acta* *48*, no. 4 605-615.
- Canfield, D. E., & Berner, R. A. (1987). Dissolution and pyritization of magnetite in anoxic marine sediments. *Geochimica et Cosmochimica Acta*, *51*(3), 645–659. [https://doi.org/10.1016/0016-7037\(87\)90076-7](https://doi.org/10.1016/0016-7037(87)90076-7)
- Calvert, S. E., & Pedersen, T. F. (1993). Geochemistry of recent oxic and anoxic marine sediments: implications for the geological record. *Marine geology*, *113*(1-2), 67-88.
- Colin, C., Turpin, L., Bertaux, J., Desprairies, A., & Kissel, C. (1999). Erosional history of the Himalayan and Burman ranges during the last two glacial–interglacial cycles. *Earth and Planetary Science Letters*, *171*(4), 647-660. [doi:10.1016/S0012-821X\(99\)00184-3](https://doi.org/10.1016/S0012-821X(99)00184-3).
- Collett, T. S., Boswell, R., Waite, W. F., Kumar, P., Roy, S. K., Chopra, K., Singh, S.K., Yamada, Y., Tenma, N., Pohlman, J. and Zyrianova, M. (2019). India National Gas Hydrate Program Expedition 02 summary of scientific results: gas hydrate systems along the eastern continental margin of India. *Marine and Petroleum Geology*, *108*, 39-142. <https://doi.org/10.1016/j.marpetgeo.2019.05.023>
- Cioppa, M. T., Porter, N. J., Trenhaile, A. S., Igokwe, B., & Vickers, J. (2010). Beach sediment magnetism and sources: Lake Erie, Ontario, Canada. *Journal of Great Lakes Research*, *36*(4), 674-685. <https://doi.org/10.1016/j.jglr.2010.07.007>

Dewangan, P., Ramprasad, T., Ramana, M. V., Mazumdar, A., Desa, M., & Badesab, F. K. (2010). Seabed morphology and gas venting features in the continental slope region of Krishna-Godavari basin, Bay of Bengal: Implications in gas-hydrate exploration. *Marine and Petroleum Geology*, 27(7), 1628-1641. <https://doi.org/10.1016/j.marpetgeo.2010.03.015>

Dewangan, P., Basavaiah, N., Badesab, F. K., Usapkar, A., Mazumdar, A., Joshi, R., & Ramprasad, T. (2013). Diagenesis of magnetic minerals in a gas hydrate/cold seep environment off the Krishna-Godavari basin, Bay of Bengal. *Marine Geology*, 340, 57-70. <https://doi.org/10.1016/j.margeo.2013.04.016>

Dillon, M., & Bleil, U. (2006). Rock magnetic signatures in diagenetically altered sediments from the Niger deep-sea fan. *Journal of Geophysical Research: Solid Earth*, 111(B3). <https://doi.org/10.1029/2004JB003540>

Esteban, L., Enkin, R. J., & Hamilton, T. (2008). Gas hydrates and magnetism: Comparative geological settings for diagenetic analysis. In ICGH. *Proceedings of the 6th International Conference on Gas Hydrates* (pp. 1-9).

Fairbanks RG, Mortlock RA, Chiu TC, Cao L, Kaplan A, Guilderson TP, Fairbanks TW, Bloom AL, Grootes PM, Nadeau MJ. (2005). Radiocarbon calibration curve spanning 0 to 50,000 years BP based on paired Th-230/U-234/U-238 and C-14 dates on pristine corals. *Quaternary Science Reviews* 24:(16-17) 1781-96. <https://doi.org/10.1016/j.quascirev.2005.04.007>

Gallaway, E., Trenhaile, A.S., Cioppa, M.T., Hatfield, R.G., (2012). Magnetic mineral transport and sorting in swash-zone: northern Lake Erie, Canada. *Sedimentology*, 59(6), 1718-1734. <https://doi.org/10.1111/j.1365-3091.2012.01323.x>

Garming, J. F. L., Bleil, U., & Riedinger, N. (2005). Alteration of magnetic mineralogy at the sulfate-methane transition: analysis of sediments from the Argentine continental slope. *Physics of the Earth and Planetary Interiors*, 151(3-4), 290-308. doi:10.1016/j.pepi.2005.04.001

Gibbs, R. J. (1977). Transport phases of transition metals in the Amazon and Yukon Rivers. *Geological Society of America Bulletin*, 88(6), 829-843. [https://doi.org/10.1130/0016-7606\(1977\)88<829:TPOTMI>2.0.CO;2](https://doi.org/10.1130/0016-7606(1977)88<829:TPOTMI>2.0.CO;2)

Hatfield, R. G., & Maher, B. A. (2008). Suspended sediment characterization and tracing using a magnetic fingerprinting technique: Bassenthwaite Lake, Cumbria, UK. *Holocene*, 18, 105-115. <https://doi.org/10.1177/0959683607085600>

Hatfield, R. G., & Maher, B. A. (2009). Holocene sediment dynamics in an upland temperate lake catchment: Climatic and land-use impacts in the English Lake District. *Holocene*, 19, 427-438. <https://doi.org/10.1177/0959683608101392>

Hatfield, R. G., Cioppa, M. T., & Trenhaile, A. S. (2010). Sediment sorting and beach erosion along a coastal foreland: Magnetic measurements in Point Pelee National Park, Ontario, Canada. *Sedimentary Geology*, 231(3-4), 63-73. <https://doi.org/10.1016/j.sedgeo.2010.09.007>

Hirt, A. M., Lowrie, W., Clendenen, W. S., & Kligfield, R. (1993). Correlation of strain and the anisotropy of magnetic susceptibility in the Onaping Formation: evidence for a near-circular origin of the Sudbury basin. *Tectonophysics*, 225(4), 231-254. doi:10.1016/0040-1951(93)90300-9

- Horng, C. S., & Chen, K. H. (2006). Complicated magnetic mineral assemblages in marine sediments offshore southwestern Taiwan: Possible influences of methane flux on the early diagenetic process. *Terrestrial, Atmospheric and Oceanic Sciences*, 17, 1009–1026. [https://doi.org/10.3319/TAO.2006.17.4.1009\(GH\)](https://doi.org/10.3319/TAO.2006.17.4.1009(GH))
- Horng, C. S. (2018). Unusual magnetic properties of sedimentary pyrrhotite in methane seepage sediments: Comparison with metamorphic pyrrhotite and sedimentary greigite. *Journal of Geophysical Research: Solid Earth*, 123(6), 4601–4617. <https://doi.org/10.1002/2017JB015262>
- Horng, C. S., & Roberts, A. P. (2018). The low-temperature Besnus magnetic transition: Signals due to monoclinic and hexagonal pyrrhotite. *Geochemistry, Geophysics, Geosystems*, 19(9), 3364–3375. <https://doi.org/10.1029/2017GC007394>
- Karlin, R., & Levi, S. (1985). Geochemical and sedimentological control of the magnetic properties of hemipelagic sediments, *J. Geophys. Res.*, 90(B12), 10373–10392, doi:10.1029/JB090iB12p10373.
- Karlin, R. (1990). Magnetite diagenesis in marine sediments from the Oregon continental margin. *Journal of Geophysical Research: Solid Earth*, 95(B4), 4405–4419. <https://doi.org/10.1029/JB095iB04p04405>
- Kars, M., & Kodama, K. (2015). Rock magnetic characterization of ferrimagnetic iron sulfides in gas hydrate-bearing marine sediments at Site C0008, Nankai Trough, Pacific Ocean, off-coast Japan. *Earth, Planets and Space*, 67(1), 118. <https://doi.org/10.1186/s40623-015-0287-y>
- Keil, R. G., Montluçon, D. B., Prah, F. G., & Hedges, J. I. (1994). Sorptive preservation of labile organic matter in marine sediments. *Nature*, 370(6490), 549–552.
- Knittel, K., & Boetius, A. (2009). Anaerobic oxidation of methane: progress with an unknown process. *Annual review of microbiology*, 63, 311–334. <https://doi.org/10.1146/annurev.micro.61.080706.093130>
- Kocherla, M., Teichert, B. M. A., Pillai, S., Satyanarayanan, M., Ramamurty, P. B., Patil, D. J., Rao, A. N. (2015). Formation of methane-related authigenic carbonates in a highly dynamic biogeochemical system in the Krishna–Godavari Basin, Bay of Bengal. *Marine and Petroleum Geology*, 64, 324–333. <https://doi.org/10.1016/j.marpetgeo.2015.02.034>
- Kumar, P., Collett, T. S., Boswell, R., Cochran, J. R., Lall, M., Mazumdar, A., Ramana, M. V., Ramprasad, T., Riedel, M., Sain, K., Sathe, A. V. (2014). Geologic implications of gas hydrates in the offshore of India: Krishna-Godavari Basin, Mahanadi Basin, Andaman Sea, Kerala–Konkan Basin. *Marine and Petroleum Geology*, 58, 29–98. <https://doi.org/10.1016/j.marpetgeo.2014.07.031>
- Krishna, K. S., Ismaiel, M., Srinivas, K., Rao, D. G., Mishra, J., Saha, D. (2016). Sediment pathways and emergence of Himalayan source material in the Bay of Bengal. *Current Science*, 363–372
- Larrasoña, J. C., Roberts, A. P., Musgrave, R. J., Gràcia, E., Piñero, E., Vega, M., Martínez-Ruiz, F. (2007). Diagenetic formation of greigite and pyrrhotite in gas hydrate marine sedimentary systems. *Earth and Planetary Science Letters*, 261(3–4), 350–366. <https://doi.org/10.1016/j.epsl.2007.06.032>
- Lee M. W., & T. S. Collett (2009), Gas hydrate saturations estimated from fractured reservoir at site NGHP-01-10, Krishna–Godavari basin, India, *J. Geophys. Res.*, 114, B07102, <https://doi.org/10.1029/2008JB006237>.

- Lees, J. A., & Pethick, J. S. (1995). Problems associated with quantitative magnetic sourcing of sediments of the Scarborough to Mablethorpe coast, northeast England, UK. *Earth Surface processes and landforms*, 20(9), 795-806. <https://doi.org/10.1002/esp.3290200905>
- Liu, Q., Roberts, A. P., Larrasoana, J. C., Banerjee, S. K., Guyodo, Y., Tauxe, L., Oldfield, F. (2012). *Environmental magnetism: principles and applications*. *Reviews of Geophysics*, 50(4).
- Maher, B. A., & R. Thompson (Eds.) (1999), *Quaternary Climates, Environments and Magnetism*, Cambridge University Press, Cambridge, U. K., doi:10.1017/CBO9780511535635
- März, C., Hoffmann, J., Bleil, U., de Lange, G. J., Kasten, S. (2008). Diagenetic changes of magnetic and geochemical signals by anaerobic methane oxidation in sediments of the Zambezi deep-sea fan (SW Indian Ocean). *Marine Geology*, 255(3-4), 118-130.
- Mazumdar, A., Joao, H. M., Peketi, A., Dewangan, P., Kocherla, M., Joshi, R. K., Ramprasad, T. (2012). Geochemical and geological constraints on the composition of marine sediment pore fluid: Possible link to gas hydrate deposits. *Marine and Petroleum Geology*, 38(1), 35–52. <https://doi.org/10.1016/j.marpetgeo.2012.07.004>
- Mayer, L. M. (1994). *Isotope Geoscienc. Chemical Geology*, 114, 347-363.
- Mohamed, K. J., Andrade, A., Rey, D., Rubio, B., Bernabeu, A. M. (2017). A kinetic model to explain the grain size and organic matter content dependence of magnetic susceptibility in transitional marine environments: A case study in Ria de Muros (NW Iberia). *Geochemistry, Geophysics, Geosystems*, 18(6), 2200-2215. doi:10.1002/2017GC006823.
- Moreno, A., Valero-Garcés, B. L., González-Sampériz, P., Rico, M. (2008). Flood response to rainfall variability during the last 2000 years inferred from the Taravilla Lake record (Central Iberian Range, Spain). *Journal of paleolimnology*, 40(3), 943-961. <https://doi.org/10.1007/s10933-008-9209-3>
- Musgrave, R. J., Bangs, N. L., Larrasoana, J. C., Gràcia, E., Hollamby, J. A., Vega, M. E. (2006). Rise of the base of the gas hydrate zone since the last glacial recorded by rock magnetism. *Geology*, 34(2), 117-120. doi: 10.1130/G22008.1
- Nagoji, S. S., & Tiwari, M. (2017). Organic carbon preservation in Southeastern Arabian Sea sediments since mid-Holocene: Implications to South Asian Summer Monsoon variability. *Geochemistry, Geophysics, Geosystems*, 18(9), 3438-3451. doi:10.1002/2017GC006804.
- Ojha, P. S., & Dubey, M. (2006). Giant hydrocarbons fields of offshore Krishna-Godavari basin, Petroview 1. Directorate General of Hydrocarbons, New Delhi, 26-30.
- Oldfield, F., & Yu, L. (1994). The influence of particle size variations on the magnetic properties of sediments from the north-eastern Irish Sea. *Sedimentology*, 41(6), 1093-1108. <https://doi.org/10.1111/j.1365-3091.1994.tb01443.x>
- Oldfield, F., Maher, B. A., Donoghue, J., Pierce, J. (1985). Particle-size related, mineral magnetic source sediment linkages in the Rhode River catchment, Maryland, USA. *Journal of the Geological Society*, 142, 1035–1046. <https://doi.org/10.1144/gsjgs.142.6.1035>
- Passier, H. D., De Lange, G. J., Dekkers, M. J. (2001). Magnetic properties and geochemistry of the active oxidation front and the youngest sapropel in the eastern Mediterranean Sea. *Geophys. J. Int.*, 145(3), 604–614. doi: 10.1046/j.0956-540x.2001.01394.x

- Peketi, A., Mazumdar, A., Pillutla, S. P. K., Rai, V. K., Sawant, B., Chaitanya, A. V. S. (2020). Monsoon rainfall and contrasting source rocks influenced sediment composition of peninsular basins along the east coast of India (western Bay of Bengal). *Marine and Petroleum Geology*, 104433. <https://doi.org/10.1016/j.marpetgeo.2020.104433>
- Peters, C., & Dekkers, M. J. (2003). Selected room temperature magnetic parameters as a function of mineralogy, concentration and grain size. *Physics and Chemistry of the Earth, Parts A/B/C*, 28(16-19), 659-667. doi:10.1016/S1474-7065(03)00120-7.
- Phillips, S. C., Johnson, J. E., Giosan, L., Rose, K. (2014). Monsoon-influenced variation in productivity and lithogenic sediment flux since 110 ka in the offshore Mahanadi Basin, northern Bay of Bengal. *Marine and Petroleum Geology*, 58, 502–525. <https://doi.org/10.1016/j.marpetgeo.2014.05.007>
- Prabhakar, K. N., & Zutshi, P. L. (1993). Evolution of southern part of Indian East Coast basin. *Journal of Geological Society of India*, 41, 215–230.
- Prajith, A., Tyagi, A., Kurian, P. J. (2018). Changing sediment sources in the Bay of Bengal: Evidence of summer monsoon intensification and ice-melt over Himalaya during the Late Quaternary. *Palaeogeography, Palaeoclimatology, Palaeoecology*, 511, 309–318. <https://doi.org/10.1016/j.palaeo.2018.08.016>
- Ramana, M. V., Ramprasad, T., Kamesh Raju, K. A., Desa, M. (2007). Occurrence of gas hydrates along the continental margins of India, particularly the Krishna-Godavari off shore basin. *International Journal of Environmental Studies*, 64(6), 675–693. <https://doi.org/10.1080/00207230701476321>
- Ramesh, R., & Subramanian, V. (1988). Temporal, spatial and size variation in the sediment transport in the Krishna River basin, India. *Journal of Hydrology*, 98, 53–65. [https://doi.org/10.1016/0022-1694\(88\)90205-3](https://doi.org/10.1016/0022-1694(88)90205-3)
- Ramprasad, T., Dewangan, P., Ramana, M. V., Mazumdar, A., Karisiddaiah, S. M., Ramya, E. R., Sriram, G. (2011). Evidence of slumping/sliding in Krishna–Godavari offshore basin due to gas/fluid movements. *Marine and Petroleum Geology*, 28(10), 1806–1816. <https://doi.org/10.1016/j.marpetgeo.2011.02.007>Rao 2001
- Rao, G. N. (2001). Sedimentation, stratigraphy, and petroleum potential of Krishna-Godavari basin, East Coast of India. *American Association of Petroleum Geologists Bulletin*, 85(9), 1623–1643.
- Razjigaeva, N. G., & Naumova, V. V. (1992). Trace element composition of detrital magnetite from coastal sediments of northwestern Japan Sea for provenance study. *Journal of Sedimentary Research*, 62(5), 802-809. <https://doi.org/10.1306/D42679E2-2B26-11D7-8648000102C1865D>
- Rey, D., Mohamed, K. J., Bernabeu, A., Rubio, B., Vilas, F. (2005). Early diagenesis of magnetic minerals in marine transitional environments: geochemical signatures of hydrodynamic forcing. *Marine Geology*, 215(3-4), 215-236. doi:10.1016/j.margeo.2004.12.001
- Riedinger, N., Pfeifer, K., Kasten, S., Garming, J. F. L., Vogt, C., Hensen, C. (2005). Diagenetic alteration of magnetic signals by anaerobic oxidation of methane related to a change in sedimentation rate. *Geochimica et Cosmochimica Acta*, 69(16), 4117–4126. <https://doi.org/10.1016/j.gca.2005.02.004>

Roberts, A. P. (2015). Magnetic mineral diagenesis. *Earth-Science Reviews*, 151, 1–47. <https://doi.org/10.1016/j.earscirev.2015.09.010>

Roberts, A. P., Zhao, X., Harrison, R. J., Heslop, D., Muxworthy, A. R., Rowan, C. J., Larrasoana, J.C. Florindo, F. (2018). Signatures of reductive magnetic mineral diagenesis from unmixing of first-order reversal curves. *Journal of Geophysical Research: Solid Earth*, 123(6), 4500–4522. <https://doi.org/10.1029/2018JB015706>.

Rodelli, D., Jovane, L., Giorgioni, M., Rego, E.S., Cornaggia, F., Benites, M., Cedraz, P., Berbel, G.B.B., Braga, E.S., Ustra, A., Abreu, F. (2019). Diagenetic fate of biogenic soft and hard magnetite in chemically stratified sedimentary environments of Mamanguá Ría, Brazil. *Journal of Geophysical Research: Solid Earth*, 124(3), 2313–2330. <https://doi.org/10.1029/2018JB016576>

Rowan, C. J., Roberts, A. P., Broadbent, T. (2009). Reductive diagenesis, magnetite dissolution, greigite growth and paleomagnetic smoothing in marine sediments: A new view. *Earth and Planetary Science Letters*, 277(1-2), 223–235. doi:10.1016/j.epsl.2008.10.016

Sangode, S. J., Sinha, R., Phartiyal, B., Chauhan, O. S., Mazari, R. K., Bagati, T. N., et al. (2007). Environmental magnetic studies on some quaternary sediments of varied depositional settings in the Indian sub-continent. *Quaternary International*, 159, 102–118. <https://doi.org/10.1016/j.quaint.2006.08.015>

Sangode, S. J., Sinha, R., Phartiyal, B., Chauhan, O. S., Mazari, R. K., Bagati, T. N., et al. (2007). Environmental magnetic studies on some quaternary sediments of varied depositional settings in the Indian sub-continent. *Quaternary International*, 159, 102–118. <https://doi.org/10.1016/j.quaint.2006.08.015>

Sangode, S. J., Suresh, N., Bagati, T. N. (2001). Godavari source in the Bengal fan sediments: Results from magnetic susceptibility dispersal pattern. *Current Science*, 660–664.

Subramanian, V. (1980). Mineralogical input of suspended matter by Indian rivers into the adjacent areas of the Indian Ocean. *Marine Geology*, 36(3-4), M29-M34. [https://doi.org/10.1016/0025-3227\(80\)90084-5](https://doi.org/10.1016/0025-3227(80)90084-5)

Thompson, R., & Oldfield, F., 1986. *Environmental magnetism*. Allen and Unwin, 227p.

Usapkar, A., Dewangan, P., Badesab, F. K., Mazumdar, A., Ramprasad, T., Krishna, K. S., Basavaiah, N. (2016). High resolution Holocene paleomagnetic secular variation records from Bay of Bengal. *Physics of the Earth and Planetary Interiors*, 252, 49–76. <https://doi.org/10.1016/j.pepi.2016.01.004>

van Dongen, B. E., Roberts, A. P., Schouten, S., Jiang, W. T., Florindo, F., Pancost, R. D. (2007). Formation of iron sulfide nodules during anaerobic oxidation of methane. *Geochimica et Cosmochimica Acta*, 71(21), 5155–5167. doi:10.1016/j.gca.2007.08.019

Vilas, F., Bernabeu, A. M., Méndez, G. (2005). Sediment distribution pattern in the Rias Baixas (NW Spain): main facies and hydrodynamic dependence. *Journal of Marine Systems*, 54(1-4), 261–276. doi:10.1016/j.jmarsys.2004.07.016

Verosub, K. L. (1977). Depositional and Post depositional Processes in the Magnetization of Sediments, *Rev. Geophys. Space Phys.*, 15 (2), 129–143. <https://doi.org/10.1029/RG015i002p00129>

Figure 1

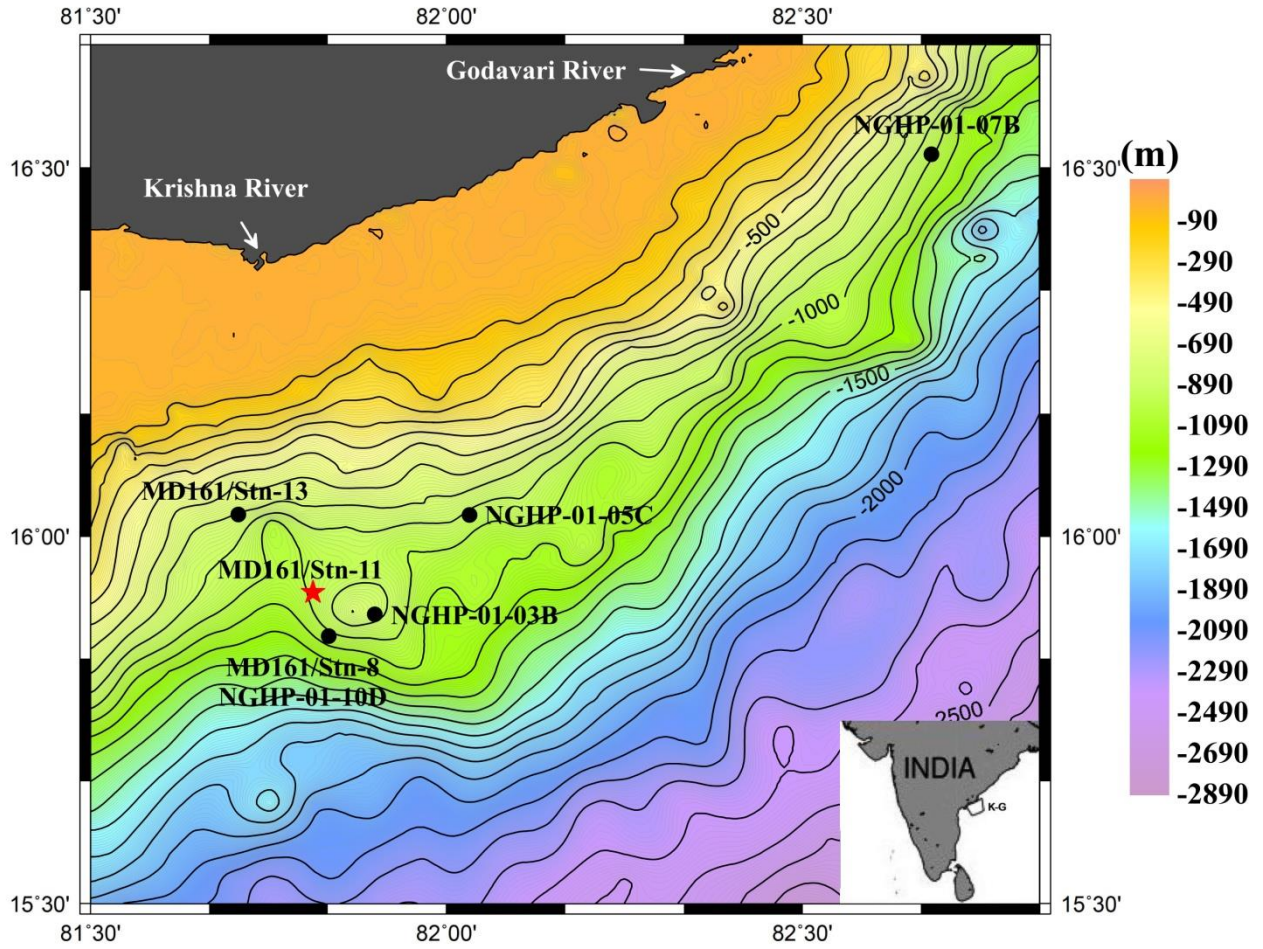


Figure 2

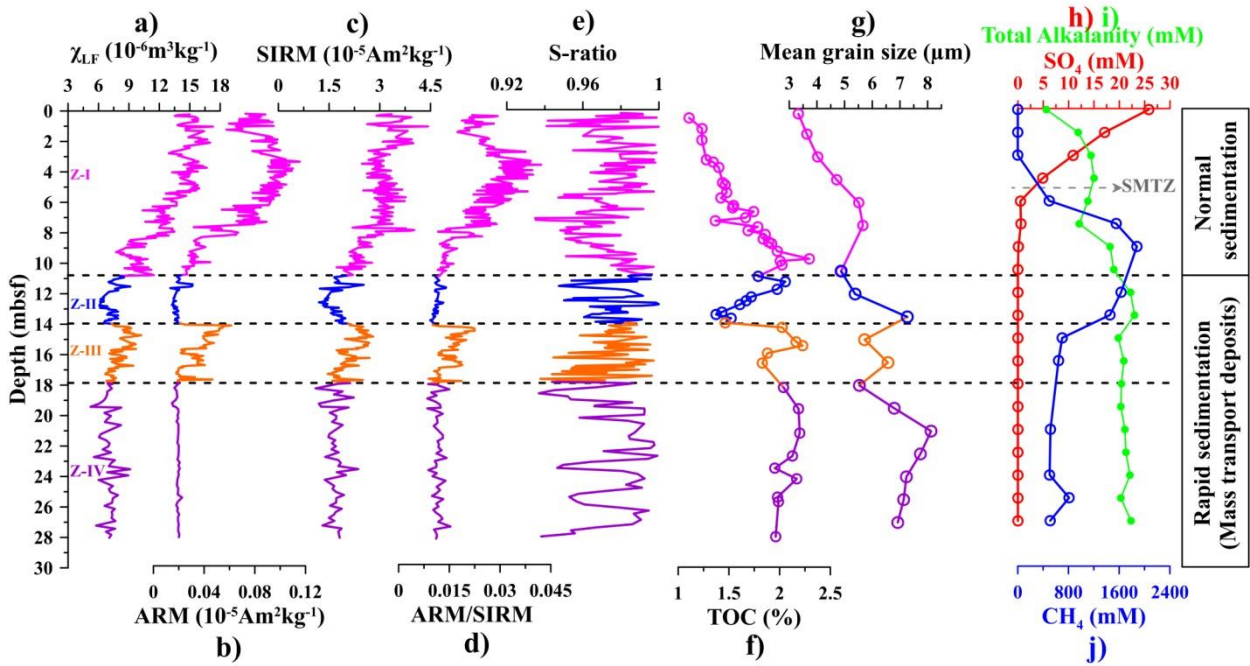


Figure 3

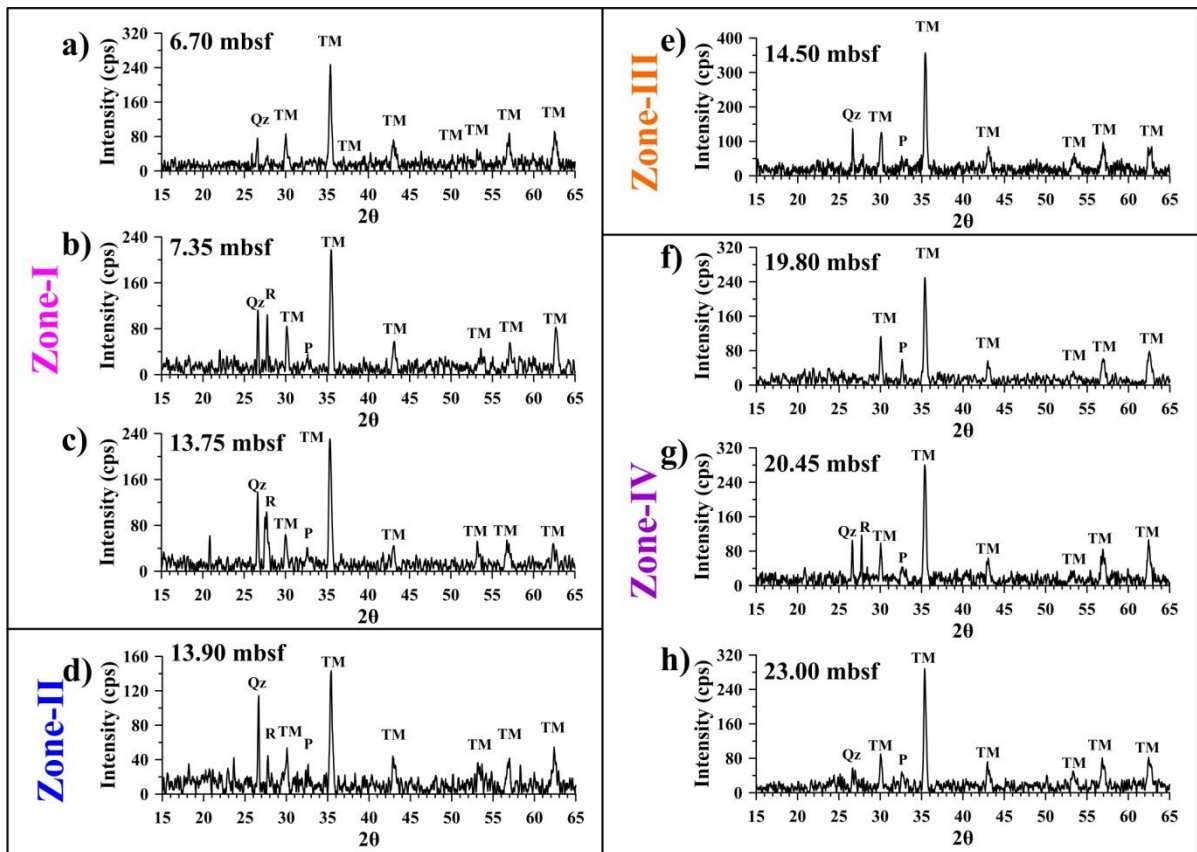


Figure 4

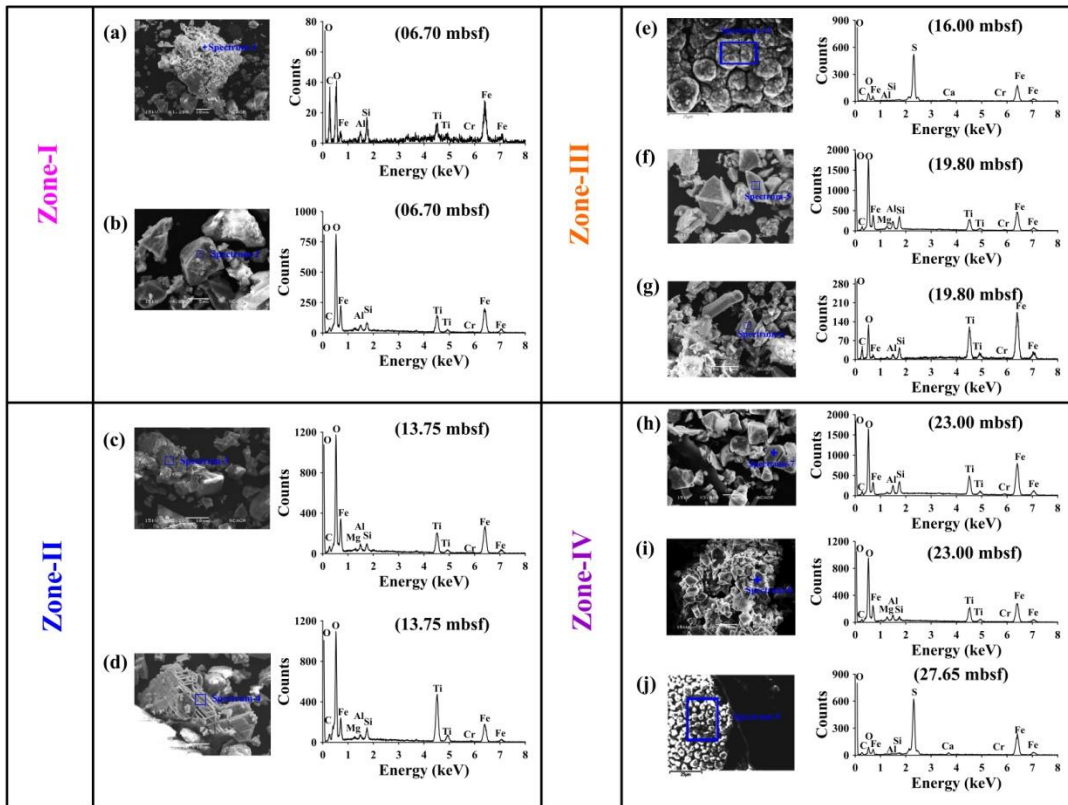


Figure 5

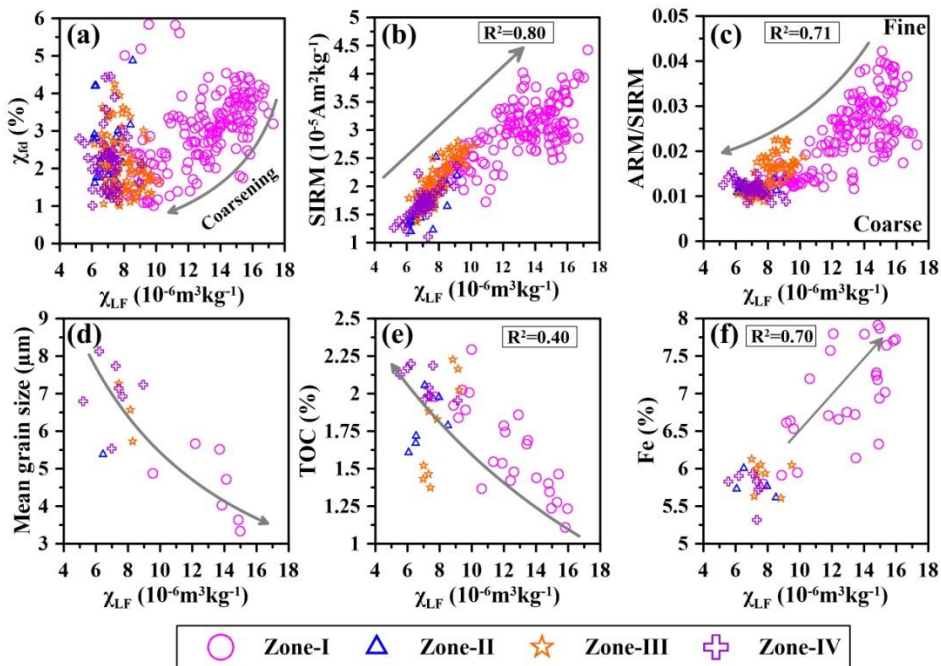


Figure 6

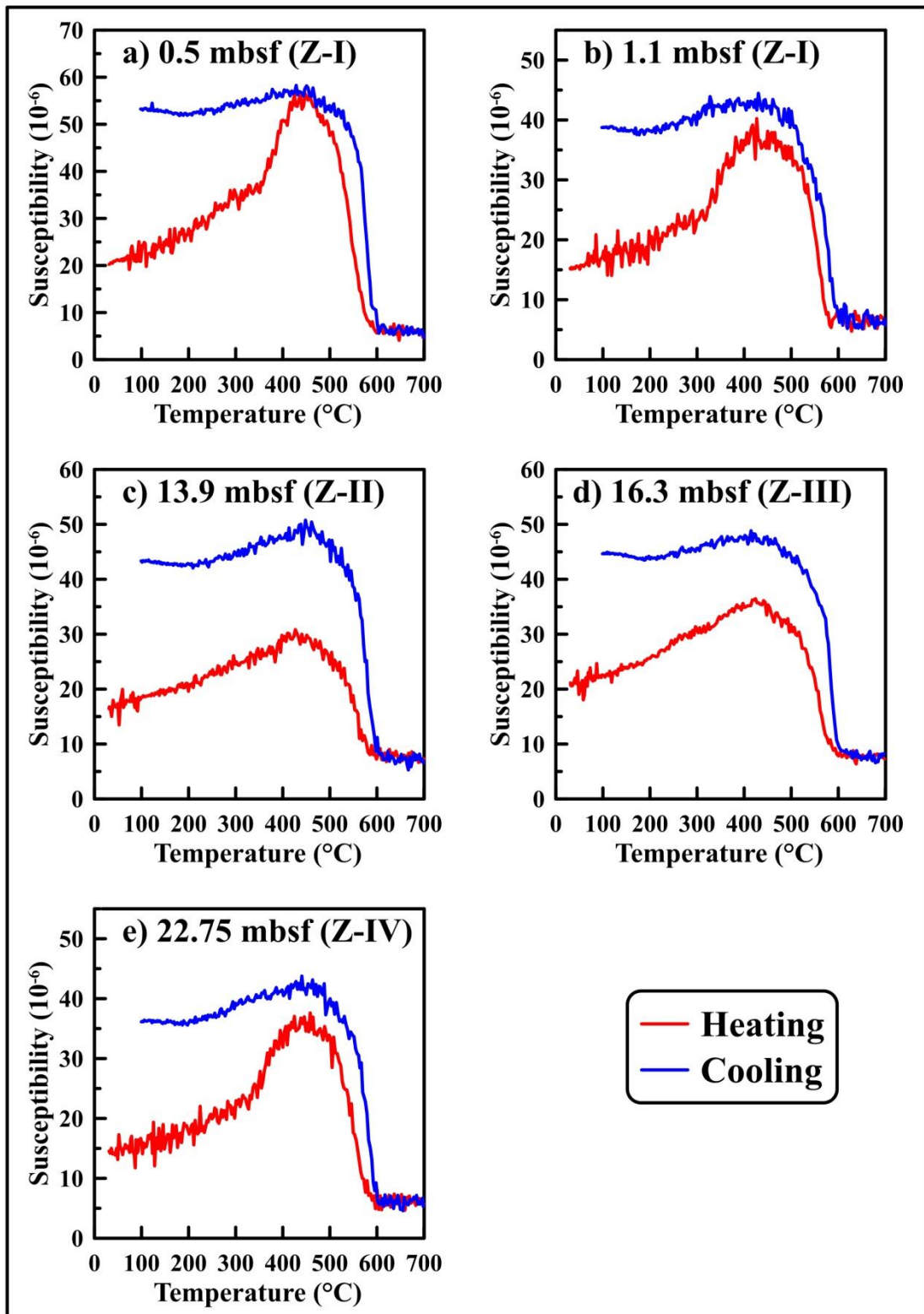


Figure 7

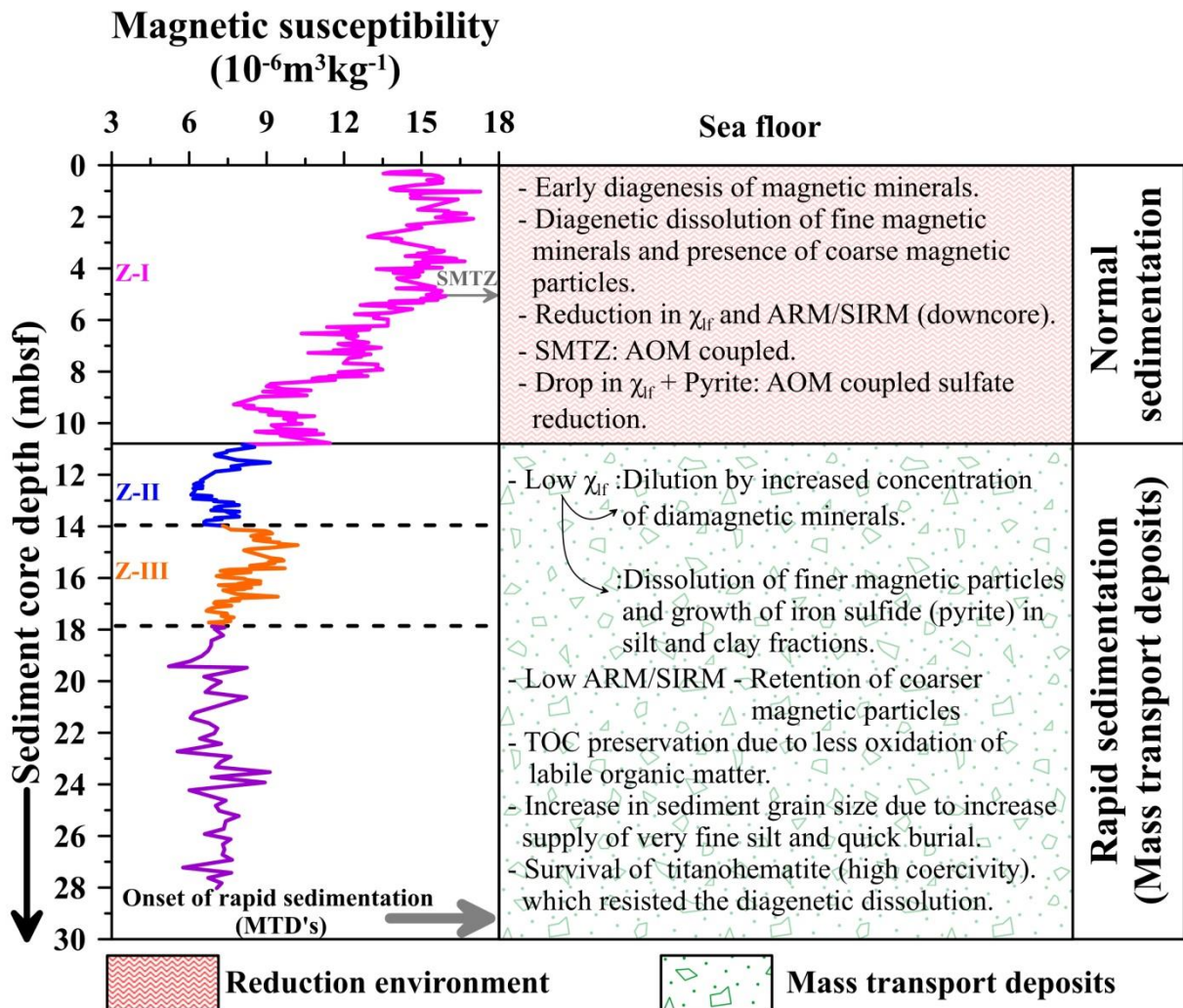


Table. 1. Calendar age of a sediment core (MD161/Stn-11; Ramprasad et al., 2011) situated in the mid-slope region of K-G offshore basin.

Sample no.	Depth (mbsf)	Calendar age (yr BP)	
		Mean	Std. dev.
MD161/Stn-11/1	0.05	648	27
MD161/ Stn-11/2	1.55	1230	36
MD161/ Stn-11/3	3.055	1677	42
MD161/ Stn-11/6	7.55	2982	61
MD161/ Stn-11/7	9.055	4163	63
MD161/ Stn-11/8	10.55	5185	98
MD161/ Stn-11/9	12.055	6296	24
MD161/ Stn-11/10	13.55	8752	111
MD161/ Stn-11/11	15.055	4700	98
MD161/ Stn-11/13	18.055	6336	43
MD161/ Stn-11/14	19.55	6258	37
MD161/ Stn-11/15	21.055	6226	69
MD161/ Stn-11/16	22.55	6333	66
MD161/ Stn-11/17	24.055	6607	55
MD161/ Stn-11/18	25.55	6327	41
MD161/ Stn-11/19	27.055	6434	48